Title: Sterols from cholesterol synthesis control distinct gene regulatory pathways

Authors: Cene Skubic[1], Hana Trček[1], Petra Nassib[1], Andrew Walakira[1], Katka Pohar[2], Sara Petek[2], Tadeja Režen[1], Alojz Ihan[2], Damjana Rozman[1*]

[1]Center for Functional Genomics and Bio-Chips, Institute of Biochemistry and molecular genetics, Faculty of Medicine, University of Ljubljana, Zaloška cesta 4, SI-1000 Ljubljana, Slovenia; [2]Institute of Microbiology and Immunology, Faculty of Medicine, University of Ljubljana, SI-1000 Ljubljana, Slovenia

*Corresponding author: Damjana Rozman

Contact information for corresponding author: Email: **damjana.rozman@mf.uni-lj.si**, Center for Functional Genomics and Bio-Chips, Institute of Biochemistry and molecular genetics, Faculty of Medicine, University of Ljubljana, Zaloška cesta 4, SI-1000 Ljubljana, Slovenia
Telephone: +386 1 543 7591

Short title: Sterols control distinct gene regulatory pathways

Funding sources: This work was funded by the Slovenian Research Agency (ARRS) program grants P1-0390, IP-022 MRIC-Elixir, MRIC-CFGBC and project grant J1-9176.

Abbreviations:

DEGs - Differentially Expressed Genes

FDR - False Discovery Rate

GSEA - Gene Set Enrichment Analysis

KEGG - Kyoto Encyclopedia of Genes and Genomes

LDS - Lipid Depleted Serum

MRM - Multiple Reaction Monitoring

TF - Transcription Factors

WB - Western Blot

Abstract

Sterol intermediates of cholesterol synthesis are largely dedicated to cholesterol. Here we assess how they influence downstream gene regulatory pathways by developing knockouts (KOs) for consecutive enzymes of cholesterol synthesis. Depletion of *CYP51*, *DHCR24* and *SC5D* resulted in accumulation of specific sterols. The overlap of deregulated genes was only 9% in terms of steroid metabolism and proliferation control, with majority of pathways changed in just one KO. The *CYP51* KO with highly elevated 24,25-dihydrolanosterol showed significantly higher proportion of cells in the G2+M phase, in line with enriched cancer and cell cycle pathways, and elevated *LEF1* by activation of WNT/NFKB/SMAD signalling. In contrast, *SC5D* and *DHCR24* KOs (with elevated lathosterol or desmosterol) slowed cell proliferation and promoted apoptosis with downregulated E2F, mitosis, cell cycle transition, and enriched HNF1A tumor suppressor. These findings demonstrate that sterols from cholesterol synthesis control distinct gene regulatory pathways, and only early sterols promote cell proliferation.

Keywords: Cholesterol/Biosynthesis, Cell signaling, Cholesterol, Cytochrome P450, Transcription, Sterols, *CYP51*, *DHCR24*, *SC5D*, LEF1

Introduction

Sterols are important lipid components of mammalian cells. Cholesterol is by far the most abundant and studied sterol molecule, being a part of cell membranes, as well as a precursor of steroid hormones, bile acids and oxysterols, all with specific downstream signalling. Cholesterol enhances membrane fluidity and decreases membrane permeability (1–3) and is involved in the formation of lipid rafts that guide many signalling pathways (4) through interaction with proteins with cholesterol binding sites (4,5). Other important roles are connected to cell division and proliferation, with sufficient cholesterol levels being necessary for cell cycle progression from G2 to the M phase (6,7). Consequently, cholesterol metabolism represents a drug targeting pathway (8,9), which can also alter other physiological processes (10) and cholesterol metabolism is also a highly oxygen-dependent process (11).

Much less is known about the functions of non-polar sterols from the late part of cholesterol synthesis (sterol intermediates) that are structurally similar to cholesterol (See Supp. Fig. S1 for detailed synthesis and individual sterol structures). Some of them, like desmosterol, can partially replace cholesterol in membranes (12), but not in lipid rafts (13). Increasing evidence supports specific roles of individual sterol intermediates. For example, some sterols have been proposed as ligands of the nuclear receptor Retinoic Acid Related nuclear receptor C (RORC; Zymostenol derivatives) and Liver X Receptor (LXR; desmosterol). Sterols also regulate protein degradation/activation of cholesterol homeostasis components, such as HMGCR (3-Hydroxy-3-Methylglutaryl-CoA Reductase), SREBF2 (Sterol Regulatory Element Binding Transcription Factor 2) and SQLE (Squalene Epoxidase) (14–17). These sterols are also control T cell differentiation (18), regulate oligodendrocyte formation (19,20), reverse protein aggregation (21) and take part in the development of hepatocellular carcinoma (22). While cholesterol is involved in the regulation of WNT signalling activities (23), the role of other sterol intermediates remains

to be determined. However in humans defects in cholesterol synthesis and consequent sterol accumulation result in severe malformations, such as are Smith-Lemli-Opitz syndrome (SLOS), Antley-Bixler syndrome, Desmosterolosis, and others. Importantly, even if in all cases the same metabolic pathway (cholesterol synthesis) is disrupted, there are dramatic differences in the disease phenotypes observed, depending on which sterols accumulate in these patients (24–27). Here we challenge the hypothesis that individual, non-polar sterol intermediates of cholesterol synthesis regulate unique sets of genes and signalling pathways that can be distinguished from their role in producing cholesterol. To investigate this, we prepared cell models in which individual genes encoding the consecutive cholesterol synthesis enzymes CYP51A1 (Cytochrome P450 Family 51 Subfamily A Member 1), DHCR24 (24-Dehydrocholesterol Reductase), SC5D (Sterol-C5-Desaturase) were disrupted by a CRISPR-Cas9 knockout targeting strategy. We performed global transcriptome analysis and applied bioinformatic tools to predict the potential binding proteins for different sterols, and validated their physiological functions in liver cells.

Materials and Methods

Preparation of knock-out cells and cell culturing

HepG2 (human liver cancer cell line, Synthego, Menalo Park, CA, USA) with CRISPR-Cas9 mediated deletion of one of the enzymes from cholesterol synthesis (CYP51A1, DHCR24 and SC5D) and the Native cell line were ordered from Synthego (Synthego, Menalo Park, CA, USA). Cells were provided as a mixed culture on which the CRISPR-Cas9 reaction was performed **(Suppl. Fig S2)** and were seeded 1 cell per well on a 96-well plate to obtain single cell colonies. Each colony was expanded, and the target gene region was PCR amplified and sequenced using Sanger sequencing (targeted regions are in **Suppl. Table S1**). The deletions that caused frameshifts (predicted with the Expasy translate tool (28)) were chosen, target gene expression measured using RT-qPCR (described in **3.3**), and protein expression tested by western blot using

specific antibodies (See **3.4**). As a final control, sterols were isolated from knock-out cell lines and sterol intermediates quantified by LC-MS/MS as described in **3.5** and **3.6** and previously by our group (29).

Cell culture condition

Cells were plated on 6-well plates and kept for 24 h in normal culturing conditions (37°C, 5% CO_2) in Dulbecco's Modified Eagle's Media (DMEM) high glucose, with 10% FBS (Fetal Bovine Serum) and 1% P/S (Penicillin-Streptomycin, all from Sigma-Aldrich®). After 24 h, culture medium was removed, cells were washed 2 times with PBS, and DMEM with 10% lipid depleted serum (Biosera inc., France) and 1% P/S with 30 µg of cholesterol (Sigma Aldrich) dissolved in 100% ethanol was added. This cell culture medium was used to reduce the effects of sterol intermediates naturally present in FBS. After 48 h in lipid depleted medium, cells were washed with PBS and RNA isolated using Tri Reagent (Sigma Aldrich) following the commercial protocol.

Gene expression analyses

For gene expression measurements all 4 cell lines (KOs and Native HepG2) were seeded on 6-well plates (1.5x10^5/well) and cultured as described in **3.2.** After 48 h in lipid depleted medium, cells were washed 2 times using 1x PBS. RNA was isolated using Tri Reagent (Sigma-Aldrich®) following the commercial protocol. RNA concentration and purity were measured using Nanodrop ND-1000 and RNA integrity (RIN) using Agilent 2100 Bioanalyses. Human Clariom™ S Assay (Thermo Fisher Scientific) microarrays were used to determine the transcriptome profiles. All KO lines were processed in triplicates. The expression of selected genes was measured by RT-qPCR (LightCycler 480; Roche), cDNA was prepared from 1 µg of RNA using QuantiNova Reverse Transcription Kit (Qiagen). SYBR Green I Master (Roche) was used for detection. Primer pairs for selected genes are listed in **Suppl. Table S2**.

Protein isolation and western blot

Total proteins were isolated using RIPA buffer; nuclear and cytoplasmic proteins were isolated according to Shreiber et al. (30). All lysis buffers were supplemented with PhosSTOP and cOmplete-mini protease inhibitor cocktail (both Roche). Protein concentration was measured by a Pierce BCA Protein Assay Kit (Thermo Scientific, USA). For protein separation Mini-PROTEAN TGX Stain-Free Precast Gels (Bio-Rad Laboratories, CA, USA) were used and then transferred to Immobilon-P PVDF Membrane (Millipore, MA, USA). For total protein normalization, No-Stain Protein Labeling Reagent (Invitrogen, MA, USA) was used to stain PVDF membrane, which was then blocked using 5% milk or BSA in TBST for 1 h at room temperature. Membranes were incubated with primary antibodies (antibodies and dilutions used are represented in **Suppl. Table S3**) overnight at 4°C, washed 3 times with TBST for 5 min and incubated with secondary antibodies for 1 h at room temperature. After washing 3 times with TBST, proteins were imaged using Immobilon Classico Western HRP substrate or Immobilon Ecl Ultra Western HRP substrate (Millipore, MA, USA) on the iBright FL1500 Imaging System (Invitrogen, MA, USA).

Sterol isolation

Sterols were isolated following the protocol described in our previous work (29). Briefly, $1x10^6$ of HepG2 cell lines (Native and 3 KO lines) were plated on a T75 culture flask for each sterol isolation (n=3 per genotype). Cells were cultured in classic DMEM medium with 10% FBS and 1% P/S. After 24 h, the cell medium was replaced with DMEM containing 10% LDS (Lipid depleted serum, Biosera inc.), 30 µg/ml cholesterol (Sigma Aldrich, Sigma Grade, ≥99%) and 1% P/S to eliminate the effect of sterol intermediates from classic FBS. After 48 h, cells were washed two times with PBS, detached using 1 mL of Trypsin (Sigma Aldrich), resuspended in 5 mL of DMEM without FBS and transferred to a 15 mL glass vial with a Polytetrafluoroethylene (PTFE) cap and cells counted for normalization. To each sample, 200 ng of internal standard Lathosterol-

D7 (Avanti Polar Lipids) was added. Isolated sterols were dissolved in 300 µl of methanol and transferred to HPLC vials.

LC-MS/MS sterol quantification

Sterol isolation and analysis was performed as described in (29). Sterols were separated on combined columns of Luna® (3 µm PFP (2) 100 Å (100 mm and 150 mm length) on a Shimadzu Nexera XR HPLC. The mobile phase consisted of 80/10/10/0.05% methanol/water/1-propanol/formic acid. HPLC was connected to a Sciex Triple Quad 3500 mass spectrometer for detection. For ionization, APCI (Atmospheric-pressure chemical ionization) was used in positive mode and detection was made in MRM (Multiple reaction monitoring) mode. The sample concentration was normalized on an internal standard (Lathosterol-d7) and sterol concentrations calculated corresponding to standards from Avanti Lipids (Avanti Polar Lipids, Alabaster, AL, USA).

Transcriptome data analysis

The quality of the raw microarray data was assessed as follows. Firstly, microarray images were visually inspected for any visible aberrations. Further quality assessment was then done using the arrayQualityMetrics function of the arrayQualityMetrics library, and the RLE (Relative Log Expression) and NUSE (normalised unscaled standard errors) functions of the oligo library. All microarrays passed the quality checks. Array data was then processed for background correction, normalisation and summarisation using the robust multichip average algorithm (rma) in the Oligo library. Differentially expressed genes were determined by linear models using the Limma Bioconductor package (Full list in **Supp. Materials Table S8-10)**. Analysis for KEGG enrichment of gene sets was performed using the clusterProfiler library. A 5% level of significance was accepted after correcting for multiple testing using the BH-FDR (Benjamini-Hochberg False Discovery Rate) method (**Supp. Materials Table S5-7**). All analyses were

performed in R v4.0.2. Data was deposited in GEO (Gene Expression Omnibus) under accession number GSE221582.

Enrichment analyses of metabolic pathways and transcription factors

For Transcription Factor Enrichment Analysis two databases were used: TRANSFAC 2.0 (31) and ChIP-x Enrichment analysis 2022 (ChEA) (32). Release 2022.2 of the TRANSFAC MATRIX TABLE was used for TRANSFAC using input lists of differentially expressed genes for each KO cell line individually. For the background sequencing file 10.000 genes for the equivalent KO with the highest p-values were used. The TRANSFAC profile Vertebrate_non_redundant_minFP was used as a matrix, and a p-value < 0.01 was used as a cut-off for statistically significant enriched TFs. Chea analysis was done using the Enrichr online tool (33,34) (https://maayanlab.cloud/Enrichr/). For each KO a list of differentially expressed genes (DEGs) was used as input. The top 20 TFs for each KO cell line are represented in **Figure 4** and a full list is presented in **Supp. materials Table S11** (Transfac), **S12, S13** and **S14** (ChEA).

Pathway enrichment analysis

The GSEA 4.1.0 (Gene Set Enrichment Analysis) method was used for pathway enrichment analysis (35,36) and results were visualized by Cytoscape software 3.8.0 (37). All parameters were used as detailed in (38). In short, a ranked gene list of all detected genes for each cell line was used as input and analysed in GSEA with 1000 permutations to obtain enriched pathways. The statistically significant (FDR<0.01) positive and negative enriched gene sets were obtained and clustered into nodes using Cytoscape and EnrichmentMap. The AutoAnotate function was used to describe the obtained clusters and then additionally manually curated. Results are illustrated in **Supp. Materials Fig. S4-6.**

Cell cycle analysis and proliferation assays

Proliferation assays were performed using Cell Counting Kit-8 (CCK8, Dojindo Molecular Technologies, Rockville, MD, USA) according to the manufacturer's protocol. Different culture

medium conditions were tested (10% FBS, 10% LDS, 10% LDS + 30 µg/ml of cholesterol) and cells were grown for up to 72 h in 6 biological replications at 5000 cell/well on a 96-well plate. After 2 h of incubation of the reagent with cells, absorbance at 450nm was measured on an Epoch Microplate Spectrophotometer (Synergy-BioTek, USA).

Cell cycle analysis was performed on 6 well plates (1.5x10^5 cells/well) in culture conditions as described in **3.2**. After 48 h in lipid depleted medium, cells were washed with PBS, harvested by trypsinization, and fixed in 70% ice-cold ethanol at 4°C for 2 h. After fixation, cells were washed and resuspended in 300 µL propidium iodide (PI) staining solution (0.1% Triton X-100, 0.1 mg/mL RNase, 0.125 µg/mL PI) for 30 min at room temperature in the dark. Cell cycle distribution was analysed using the BD FACSCanto II system (BD Biosciences, San Jose, California, US), with the BD FACSDiva™ software (BD Biosciences, San Jose, California, US). The assay was repeated in 3 independent measurements each time in 6 technical repeats (n=6).

Statistical analysis of WB, RT-qPCR, Cell cycle and Proliferation data

To evaluate results obtained from different cell lines, a one-way ANOVA test was used with multiple comparison against the Native cell line. The significance levels were defined as: * $p < 0.05$, ** $p < 0.01$, *** $p < 0.001$, and **** $p < 0.0001$. Unless otherwise stated results are presented as mean +/- standard deviation (error bars). Analysis and visualization were performed in GraphPad Prism 9 (GraphPad Software, San Diego, CA, USA). The statistics for microarray data, enrichment analyses and pathway enrichment analysis were performed separately as described. Venn diagrams were prepared using the Venny 2.1.0 platform (https://bioinfogp.cnb.csic.es/tools/venny/index.html).

Results

Targeting cholesterol synthesis

CRISPR-Cas9 generated deletion of selected genes from the late part of cholesterol synthesis (*CYP51A1, DHCR24, SCD*5), as described in Methods. HepG2 single-cell clones were initially validated at the DNA level from colonies with identical changes on both alleles (homozygous change of the gene in the DNA sequence). The detailed DNA changes, with the positions of the deletions/insertions, the guide sequences for individual gene targeted by CRISPR-Cas9 and their predicted effects on protein sequences are shown in **Supp. data, Table S1**. The selected colonies were then tested at the mRNA and protein levels (**Figure 1**). For the *CYP51* and *DHCR24* genes, an early stop codon was predicted (**Table S1**) and we were able to completely eliminate mRNA expression and consequently protein levels of CYP51A1 (**Figure 1 A, D**) and DHCR24 (**Figure 1 B, E**). In the case of targeting the *SC5D* gene, we introduced a 2bp deletion on both alleles, which did not result in a stop codon; consequently, mRNA and protein were still present (**Figure 1C, F**). Nevertheless, changes in amino acid sequence and changes in the open reading frame resulting in a non-functional SC5D enzyme were predicted, which was further validated by sterol analysis (**Figure 1 J**).

Accumulation of sterols upon targeted inactivation of genes from cholesterol synthesis

Sterols successfully isolated and quantified by LC-MS are represented in **Figure 1 J)** and in **Supp. Fig. S3**, where, for each genotype, the proposed state of cholesterol synthesis is depicted. In the Native HepG2 cell line, we detected and quantified all measured sterol molecules except FF-MAS. In the *CYP51* KO cells, we detected an elevated concertation of lanosterol (1277 ng/10^7 cells, ~30x fold increase compared to Native) and extremely elevated concertation of 24,25-dihydrolanosterol (31 µg/10^7 cells, ~1500x fold change compared to Native). No other sterols

were present, additionally confirming successful *CYP51* deletion. In the *DHCR24* KO, sterols from the Kandutsch-Russell pathway are absent and sterols from the Bloch synthesis pathway are accumulated with approximate fold changes compared to Native of ~3x lanosterol, ~7x T-MAS, ~10x Zymosterol, ~18x 24-dehydrolathosterol, ~50x 7-dehydrodesmosterol, and the most abundant ~300x desmosterol as a final step of the synthesis. The latter clearly indicates accumulation of all sterols of the Bloch pathway with higher concentrations towards the final synthesis steps. In cells with a *SC5D* deletion only zymosterol (~8x fold change) and lathosterol (~75x fold change) were seen in high concentrations, but this was not seen for earlier sterols nor sterols from the Bloch pathway, probably due to high DHCR24 enzyme activity. Since cholesterol cannot be synthesised, the cholesterol measured **Figure 1 J)** is from the culture medium. Cholesterol originates from cell synthesis only in Native cells, in which its concentration is 2-3 times higher compared to KO cell lines. While HMGCR (**Figure 1 G**) is only elevated in *SC5D* KO, both cytoplasmic and nuclear form of SREBP2 protein are not elevated but even lowered especially in *SC5D* KO (**Figure 1 H, J**), suggesting that disrupted cholesterol synthesis, did not directly activate its synthesis pathway through SREBP2 mediated HMGCR upregulation.

Gene expression profiling, transcription factor enrichment and pathway enrichment analysis

After measuring the transcriptome using Clarium S Arrays and statistical analysis, differentially expressed genes (DEGs) lists (adj pvalue <0.05) for each KO cell line were obtained (full list in **Supp. materials Table S5-7**). All genes were used for the PCA plot (**Figure 2 A**), on which the three KO cell lines cluster separately and away from the Native HepG2 cells. Compared to the HepG2 Native cell line there were 411 DEGs in *CYP51* KO, 542 DEGs in *DHCR24* KO and 765 DEGs in *SC5D* KO **(Figure 2 B)**. Comparison of DEG lists between the three genotypes showed only 107 DEGs (or 8.9% of total) that are common to all genotypes. Between 5-10% of genes are

common to two KO lines, but more than 65% of total DEGs are changed just in one of the KO cells **(Figure 2 C)**. Differences between genotypes in DEGs indicate that production of cholesterol is not the main trigger for genes being expressed, but is most likely a consequence of accumulation of specific sterols and their signalling. To find the differences in sterol signalling, it is important to identify genes with very high log fold change (logFC) that are differentially expressed in just one genotype. In *CYP51* KO *CDH2* (N-Cadherin) is downregulated with a logFC of -3.4 (compared to logFC of -0.8 in *DHCR24 KO* and unchanged in *SC5D KO*). In the *DHCR24 KO*, *CPNE8* and *OXCT1* are highly downregulated, while *FREM1* is upregulated. In the *SC5D KO* the *ZNF385B* gene involved in the promotion of apoptosis by TP53 factor (39) is extremely upregulated with a logFC of 4.8, while unchanged in *CYP51 KO* and *DHCR24* KO.

KEGG metabolic pathway analysis showed that more than half of the pathways were significantly changed just in one of the KOs (**Figure 2 D)**. These pathways are indicated with **#** in **Figures 2 H, I, J**. Insulin resistance, ECM-receptor interaction, NF-kappa B and PI3K-Akt signalling are modulated just in the *CYP51 KO* cell line. FoxO, Insulin and Apelin signalling are changed just in *DHCR24* KO, while Biosynthesis of unsaturated fatty acids, Fatty acid metabolism, Cellular senescence and PPAR signalling pathways are a hallmark of the *SC5D* KO cell line, with Fatty acid metabolism genes like *FADS2*, *ELOVL6*, *HSD17B12* and *CYP2J2* upregulated. The commonly modulated pathways, changed in at least two KOs, are mostly linked to disturbed cholesterol synthesis, like Steroid biosynthesis and Bile secretion.

For enriched transcription factor analyses, we applied two methods that use different approaches to propose transcription factor gene regulatory networks based on differentially expressed genes and pathways: Transfac 2.0 (31) and ChEA (40). These returned different sets of TFs enriched in KOs cell lines. The top enriched TFs from both analyses are presented in **Figure 3, B and D)** (full list in **Supp. S11-S14**). Based on the ChEA analysis **(Figure 3 A, B)** the TF with the lowest p-value in all KOs was FOXA2 (also HNF3B), which regulates bile acid metabolism and is

associated with ER stress (41,42). Nuclear receptors enriched in all KOs were: LXR (Liver X Receptor), PPARA (Peroxisome Proliferator Activated Receptor Alpha) and RXR (Retinoid X Receptor), which are known to act as heterodimers and regulate hepatic lipid homeostasis (43,44). Sterol intermediates and oxysterols were proposed as LXR agonists, with desmosterol being the main sterol agonist, while lanosterol appears not to affect LXR activation (45–47). The *DHCR24* KO with a high desmosterol concentration had the highest LXR enrichment (lowest p value). Our data also indicate activated LXR in *CYP51* KO where just lanosterol and 24,25-dihydrolanosterol are present. Based on previous studies it is unlikely that either lanosterol would activate LXR, but probably some secondary oxysterols or bile acids originating from accumulated (24,25-dihydro) lanosterol do so.

Transfac analysis showed TRIM28, TFAP2A, KLF6 and E2F as the main TFs enriched in all KO cell lines with KLF6 and E2F1 also enriched in the *SC5D* KO in ChEA analysis. KLF6 (Kruppel-like factor 6) is a known tumour suppressor factor that suppress cell proliferation in a TP53-independent manner (48), while E2F1 can promote proliferation and/or apoptosis (49). Complementary to KEGG pathway analysis (Figure 2 H), NFKB1 (Nuclear Factor Kappa B Subunit 1) is enriched in both datasets in the *CYP51* KO (Figure 3 A, C), which strongly indicates the potential role of 24,25-dihydrolanosterol (**Figure 1**) in the activation of the NFKB pathway. NFKB regulates the expression of genes involved in cancer development and progression, such as proliferation, migration, and apoptosis (50). The TFs enriched mainly just in the *CYP51* KO (Figure 3 B, D) are connected to proliferation control – ESR1, STAT3, NANOG and especially TP53 (51–54), together with NFKB, indicate changes in cell growth control in *CYP51* KO. LEF1 (lymphoid enhancer binding factor 1), enriched in *CYP51* KO and *DHCR24* KO, is a part of WNT signalling, connected to increased cell proliferation, epithelial-mesenchymal transition and cancer progression (55–57). Its mRNA and protein levels were highly elevated in the *CYP51* KO, as discussed later. The *CYP51* and *DHCR24* KOs also share enriched CJUN and NR1I2 (also

PXR-pregnane X receptor) TFs. The TFs that were mainly enriched in the *DHCR24* KO (Figure 3 B, D) are NR3C1 (also GR-Glucocorticoid Receptor), HNF1A, TP63, and OLIG2. The latter activates the expression of myelin-associated genes that are normally expressed only in brain tissue and not in the liver. The enrichment of OLIG2 is interesting in the context of recent discoveries showing that 8,9-unsaturated sterols can drive oligodendrocyte formation and remyelination. (19). The *DHCR24* KO uniquely shows 8,9-accumulation of unsaturated sterols, such as zymosterol, TMAS, and probably other sterol molecules that were not measured in our LC-MS run (**Figure 1**), and enrichment of OLIG2, confirming the specific function of this group of sterol intermediates. With the largest number of DEGs, the *SC5D* KO has the highest number of unique enriched TFs. These are: XBP1 an ER stress-related TF active in the unfolded protein response (58), possibly resulting due to errors in SC5D protein folding; SREBF1/2 a TF responsible for regulation of genes responsible for uptake of cholesterol, fatty acids, triglycerides, and phospholipids (59); CCND1 (Cyclin D1), which controls G1/S cell phase transition (60); and EGR1 (early growth response-1) which regulates several tumour suppressor factors and inhibits cell proliferation (61). Similar results were obtained from pathway enrichment analysis **(Supp. Fig S4, S5** and **S6)**. In the *CYP51* KO (**Supp. Fig S4**) processes involved in immune response and higher cell proliferation are upregulated, whereas these pathways that enable successful cell division are downregulated in the *DHCR24* (**Supp. Fig S5)** and *SC5D* KOs **Supp. Fig S7)**.

Sterols modulate cell proliferation and cell cycle

Based on the transcription factor gene regulatory networks and pathway analysis, we expected major changes in proliferation and cell cycle phase in KO cells. Proliferation assays were performed under three different culture medium conditions (see also **Supp. Fig. S7**) represented in **Figure 4**: classic 10% FBS **(A)**, 10% LDS + 30 µg/ml cholesterol **(B)** and 10% LDS **(C)** (LDS- Lipid Depleted Serum – sterol concentrations from both FBS and LDP are shown in **Supp. Table S4**). In FBS, which contains cholesterol and sterol intermediates, no statistically significant

difference in proliferation of KO cells was observed compared to Native cells. However, *CYP51* KO cells grew faster compared to *DHCR24* (p=0.0011) and *SC5D* KOs (p=0.0026) at the 72 h time point (significance not indicated on **Figure 4 A)**. In both conditions using LDS instead of FBS (**Figure 4 B, C)**, *DHCR24* KO and *SC5D* KO proliferation slowed significantly at 48 h and 72 h, but *CYP51 KO* cells grew at the same speed as Native cells. Especially interesting is the fact that although the KO cells cannot synthesise cholesterol *CYP51* KO cells seem to grow normally for 72h in culture medium with lipid depleted serum, which only has trace amount of cholesterol. This is not the case for *DHCR24* KO and *SC5D* KO, where the accumulated sterols (**Figure 1**) are structurally more similar to cholesterol (especially in the *DHCR24* KO) and can replace cholesterol to some degree (12). 24,25-dihydrolansterol and lanosterol are the first sterols in cholesterol synthesis, structurally most different from cholesterol and can in principle not substitute cholesterol in membranes. Cell cycle analysis (**Figure 4 D)** confirms the result from the proliferation assay. Compared to Native the *DHCR24* KO and especially the *SC5D* KO have a higher percentage of cells in G0+G1 cell phase (58% for Native cells compared to 63% for the *DHCR24* KO and 68% for the *SC5D* KO*)*, while *CYP51* KO (57 %) does not differ from Native in the G0+G1 phase (**Figure 4 E)**. All KOs have a statistically significantly lower percentage of cell in S phase, with the lowest in *SC5D* KO cells. Differences between KOs are again seen in G2+M, where compared to the Native (24 %), *DHCR24* KO (22 %) and *SC5D* KO (20 %) have lower, but *CYP51* KO (28 %) a significantly higher percentage of cells in G0+M phase. This is consistent with the above results showing slower growth of *DHCR24* KO and *SC5D* KO cell lines. Also in concordance are the data from the transcription factor gene regulatory networks and pathway enrichment analysis (**Supp**. **Fig. S4-6),** where in *CYP51* KO proliferation pathways are upregulated and in *DHCR24* and *SC5D* KOs pathways like E2F, mitosis and regulation of cell cycle, and cell cycle transition are downregulated. In *DHCR24* and *SC5D* KOs TF HNF1A, which acts as tumour suppressor (62), is enriched.

Upregulation of LEF1 by activation of WNT/NFKB/SMAD pathway

Measuring the first 40 RORC target genes obtained from (63) **Figure 5 A)** did not indicate changes that would depend on the sterols accumulating in specific KO cell line. Especially, desmosterol and zymosterol (14,18) are known RORC agonists, and we expected upregulation of RORC target genes in *DHCR24* and *SC5D* KOs and downregulation in *CYP51* KO, where these sterols are absent, but we were not able to confirm this. Using overexpression of *RORC*, immunoprecipitation and LC-MS (**Supp. Fig S9**) we aimed to isolate and quantify sterols bound to RORC protein in our cell models. However, this proved to be experimentally difficult also due to the nature of non-polar sterols. Most data on sterol-RORC interactions was obtained on Th17 thymocytes on RORC isoform 2 (RORgt) (14,18), while in the liver the predominant isoform is RORC1 (64), which may not have the same ligand affinity.

However, we did uncover the role of sterols in the WNT signalling pathway. **Figure 5 B)** shows differential gene expression from the WNT signalling pathway (obtained from the KEGG pathway database, PATHWAY: map04310) as detected by microarray analysis with selected WNT genes measured by RT-qPCR shown in **Figure 5 C**. Interestingly *DKK4* is highly upregulated in all KOs. *DKK1* is upregulated in *DHCR24* KO and downregulated in the other two KOs, both of them being WNT pathway antagonists (65). Another WNT antagonist is *TLE4* (66) which is highly upregulated in *SC5D* KO. The mRNA expression of *LEF1* as the key transcription factor of WNT signalling is moderately elevated in *DHCR24* KO and extremely elevated (17x fold change) in *CYP51* KO, but unchanged in the *SC5D* KO. Western blot (**Figure 5 D**, **E)** shows LEF1 protein detected only in *CYP51* KO, in high quantity. Transcription factors LEF1 and TCFs (T-cell factors, not changed on mRNA level, data not shown) are the main effectors of WNT signalling, whose transcription is regulated by β-catenin (CTNNB1). When the

WNT pathway is active β-catenin stops being translocated to proteasomes for degradation. Instead it is translocated to the nucleus where it binds the LEF1/TCF promoter region (**Figure 6**). N-cadherin (CDH2), whose mRNA is downregulated (logFC of -3.4) in *CYP51* KO can bind to the AXIN1-LRP6 complex and promote β-catenin degradation (67). Looking at WNT signalling proteins (**Figure 5 D)** revealed that majority of them are unchanged (WNT5a/b, DVL3, LRP6, phosphorylated-LRP6 and Naked1). AXIN1 and cytoplasmic β-catenin were lower in *CYP51 KO*, which could indicate active state of WNT signalling, but nuclear fraction of β-catenin did not show changes. While accumulation of desmosterol, lathosterol, and other downstream sterols caused some changes in WNT genes, the LEF1 protein was not expressed. These data clearly indicate that accumulation of 24,25-dihydrolansterol caused high transcription and translation and (based on TFs enrichment) also activation of LEF1, which is known to promote cell proliferation like that seen in *CYP51* KO cells (55,57). Recent research (68), has shown an opposite effect of sitosterol, which lowers cell proliferation through blockage of WNT-LEF1 pathway. This confirms that different sterols have unique and sometimes opposite effects on LEF1 signalling.

Outside the WNT pathway, *LEF1* is regulated by the SMAD and NFKB TFs, both enriched in *CYP51* KO (69). NFKB can be activated canonically through different receptors like TLRs, RANK, CD30, CD40 and TNG-α or by an alternative pathway through LTβR, CD40 and BAFF-R receptors (discussed in more detail in (70)). The NFKB pathway regulates *LEF1* by direct binding of NFKB to the *LEF1* promoter region (**Figure 6**) (69,71). Besides *LEF1*, DEGs regulated by activated NFKB in *CYP51* KO and connected to the Immune response (a group of pathways changed in GSEA analysis **Supp. Fig**. **S4**) are *IL-18*, *ICAM-1*, *ICAM2 C3*, and *LYN*. The third mechanism by which *LEF1* expression is controlled is by the SMAD TFs, which are part of the TGFβ pathway. This is not enriched in our data set, but both SMAD2 and SMAD3 are enriched in ChEA analysis (72). There are some indications, that the TGFβ and WNT pathways can cooperatively regulate *LEF1* (73) and considering that WNT and NFKB can also crosstalk

and regulate *LEF1* (74), changes in LEF1 resulting from 24,25-dihydrolanosterol could emerge via one or more of these pathways.

Discussion

Using CRISPR-Cas9, we obtained cell lines with KOs in one of the three genes from the late part of cholesterol synthesis (75,76) – *CYP51*, *DHCR24* and *SC5D*. This resulted in non-functional enzymes and an accumulation of sterols upstream of the deleted enzymes, with depleted sterols downstream. All KO cells were unable to synthesise cholesterol. In humans, all errors in the late part of cholesterol synthesis result in mental and physical defects, generally being more severe at the beginning of the post-lanosterol part of synthesis (24). In mouse models, whole body CYP51A1 deletion was embryonically lethal (77). Deletion only in the liver resulted in lanosterol and 24,25-dihydrolansterol accumulation, which led to tumour growth and hepatocellular carcinoma-like symptoms (22,78). Much of our findings in HepG2 *CYP51* KO cells, where especially 24,25-dihydrolansterol concentration are high, aligns with results in mouse models (22), where signalling pathways such as NFKB, PI3K/Akt, and the cell cycle are altered. A similar observation was recently made by Sax et al. (79), where they performed high-throughput small-molecule screens and tested oligodendrocyte formation. They observed a higher number of living cells and higher proliferation in cells treated with amorolfine, an inhibitor of CYP51A1 and EBP enzymes. This is consistent with our results, in which deletion of *CYP51* and accumulation of lanosterol and 24,25-dihydrolansterol resulted in HepG2 cells having a higher percentage of cells in G2+M and the same proliferation level as Native cells even in conditions with lower cholesterol content in the medium. Higher proliferation in *CYP51 KO* might be explained by high expression of *LEF1*, which promotes cell proliferation and has oncogene potential (56). *LEF1* can be activated through the WNT pathway, by activation of NFKB (74) or by SMADs TFs (69).

Transcription was enriched in all KOs but in *SC5D* and *DHCR24* KO*s* proliferation was significantly lower and more cells were in G0 phase. In cells with higher concentration of downstream sterols, especially desmosterol in *DHCR24* KO and lathosterol in *SC5D* KO, the sterols caused slower proliferation rates and more cells accumulating in G0/1 phase. Although it is not possible to establish beyond doubt that the lower proliferation and cell cycle changes are caused by sterols downstream of zymosterol rather than by lower cholesterol levels, which depletion can both promote or inhibit proliferation (80,81), the downstream sterols appear to have a direct effect on cell cycle regulation and proliferation. A possible mechanism is through TFs like factor E2F, which plays a crucial role in the cell cycle control and apoptosis, (82) and HNF1A which supresses proliferation (62). Interestingly, lathosterol accumulation in *SC5D* KO caused upregulation of fatty acid metabolism pathways and PPAR signalling. This requires clarification. Sterols from the Bloch pathway, especially desmosterol in *DHCR24* KO, caused enrichment of OLIG2, a TF usually found in the brain promoting myelination. This is interesting in the context of previously published work where it was shown that 8,9-unsaturated sterols caused remyelination of oligodendrocytes (19). From our experiments we were unable to confirm that sterols like desmosterol and zymosterol bind to RORC or activate nuclear receptor RORC as was shown previously for other cell types (14,18). The reason could be that this sterol-RORC interaction does not occur in hepatocytes, more specifically in the HepG2 cell line, or that RORC transcriptional activity was lower compared to other transcriptomic changes caused by sterols in KO cells. Our findings, together with previous work, clearly show that sterols from the late part of cholesterol synthesis have distinct biological functions and regulate distinct downstream gene regulatory pathways. Importantly, only early sterols can promote cell proliferation, with 24,25-dihydrolanosterol having the biggest effect, while sterols from the end of cholesterol synthesis suppress proliferation. Further studies with focus on individual sterols are needed, to improve the mechanistic insight into how sterols regulate different cellular processes.

Data availability statement

Data was deposited in GEO (Gene Expression Omnibus) under accession number GSE221582.

Acknowledgments

We thank John Hancock for reviewing the English language in the final manuscript.

References

1. Simons K, Ikonen E. How cells handle cholesterol. Science [Internet]. 2000 Dec;290(5497):1721–6. Available from: doi:10.1126/science.290.5497.1721

2. Brown AJ, Sharpe LJ. Cholesterol Synthesis [Internet]. Sixth Edit. Biochemistry of Lipids, Lipoproteins and Membranes: Sixth Edition. Elsevier; 2016. 327–358 p. Available from: http://dx.doi.org/10.1016/B978-0-444-63438-2.00011-0

3. Skubic C, Rozman D. Sterols from the Post-Lanosterol Part of Cholesterol Synthesis: Novel Signaling Players. In: Rozman D, Gebhardt R, editors. Mammalian Sterols : Novel Biological Roles of Cholesterol Synthesis Intermediates, Oxysterols and Bile Acids [Internet]. Cham: Springer International Publishing; 2020. p. 1–22. Available from: https://doi.org/10.1007/978-3-030-39684-8_1

4. Pike LJ. Lipid rafts: Bringing order to chaos. J Lipid Res [Internet]. 2003;44(4):655–67. Available from: http://dx.doi.org/10.1194/jlr.R200021-JLR200

5. Bukiya AN, Dopico AM. Common structural features of cholesterol binding sites in crystallized soluble proteins. J Lipid Res. 2017;58(6):1044–54.

6. Fernández C, Lobo M del VT, Gómez-Coronado D, Lasunción MA. Cholesterol is essential for mitosis progression and its deficiency induces polyploid cell formation. Exp Cell Res [Internet]. 2004;300(1):109–20. Available from: https://www.sciencedirect.com/science/article/pii/S0014482704003854

7. Rodríguez-Acebes S, de la Cueva P, Fernández-Hernando C, Ferruelo AJ, Lasunción MA, Rawson RB, et al. Desmosterol can replace cholesterol in sustaining cell proliferation and regulating the SREBP pathway in a sterol-Δ 24-reductase-deficient cell line. Biochem J. 2009;420(2):305–15.

8. Ogura S, Yoshida Y, Kurahashi T, Egawa M, Furuta K, Kiso S, et al. Targeting the mevalonate pathway is a novel therapeutic approach to inhibit oncogenic FoxM1 transcription factor in human hepatocellular carcinoma. Oncotarget. 2018;9(30):21022–35.

9. Yang J, Wang L, Jia R. Role of de novo cholesterol synthesis enzymes in cancer. J Cancer. 2020;11(7):1761–7.

10. Wages PA, Kim H-YH, Korade Z, Porter NA. Identification and characterization of prescription drugs that change levels of 7-dehydrocholesterol and desmosterol. J Lipid Res [Internet]. 2018;59(10):1916–26. Available from: https://www.sciencedirect.com/science/article/pii/S0022227520341833

11. Coates HW, Capell-Hattam IM, Olzomer EM, Du X, Farrell R, Yang H, et al. Hypoxia truncates and constitutively activates the key cholesterol synthesis enzyme squalene

monooxygenase. Elife. 2023;12:1–26.

12. Huster D, Scheidt HA, Arnold K, Herrmann A, Müller P. Desmosterol may replace cholesterol in lipid membranes. Biophys J. 2005;88(3):1838–44.

13. Vainio S, Jansen M, Koivusalo M, Róg T, Karttunen M, Vattulainen I, et al. Significance of sterol structural specificity: Desmosterol cannot replace cholesterol in lipid rafts. J Biol Chem. 2006;281(1):348–55.

14. Santori FR, Huang P, Van De Pavert SA, Douglass EF, Leaver DJ, Haubrich BA, et al. Identification of Natural RORg Ligands that Regulate the Development of Lymphoid Cells. Cell Metab [Internet]. 2015;21(2):286–97. Available from: http://dx.doi.org/10.1016/j.cmet.2015.01.004

15. Chen L, Ma MY, Sun M, Jiang LY, Zhao XT, Fang XX, et al. Endogenous sterol intermediates of the mevalonate pathway regulate HMGCR degradation and SREBP-2 processing. J Lipid Res. 2019;60(10):1765–75.

16. Muse ED, Yu S, Edillor CR, Tao J, Spann NJ, Troutman TD, et al. Cell-specific discrimination of desmosterol and desmosterol mimetics confers selective regulation of LXR and SREBP in macrophages. Proc Natl Acad Sci U S A. 2018;115(20):E4680–9.

17. Nakamura Y, Sakakibara J, Izumi T, Shibata A, Ono T. Transcriptional Regulation of Squalene Epoxidase by Sterols and Inhibitors in HeLa Cells (*). J Biol Chem [Internet]. 1996;271(14):8053–6. Available from: https://www.sciencedirect.com/science/article/pii/S0021925817456055

18. Hu X, Wang Y, Hao LY, Liu X, Lesch CA, Sanchez BM, et al. Sterol metabolism controls TH17 differentiation by generating endogenous RORγ agonists. Nat Chem Biol [Internet].

2015;11(2):141–7. Available from: http://dx.doi.org/10.1038/nchembio.1714

19. Hubler Z, Allimuthu D, Bederman I, Elitt MS, Madhavan M, Allan KC, et al. Accumulation of 8,9-unsaturated sterols drives oligodendrocyte formation and remyelination. Nature [Internet]. 2018 Aug;560(7718):372–6. Available from: http://dx.doi.org/10.1038/s41586-018-0360-3

20. Pleshinger MJ, Friedrich RM, Hubler Z, Rivera-León AM, Gao F, Yan D, et al. Inhibition of SC4MOL and HSD17B7 shifts cellular sterol composition and promotes oligodendrocyte formation. RSC Chem Biol. 2021;

21. Zhao L, Chen X-J, Zhu J, Xi Y-B, Yang X, Hu L-D, et al. Lanosterol reverses protein aggregation in cataracts. Nature [Internet]. 2015;523(7562):607–11. Available from: https://doi.org/10.1038/nature14650

22. Cokan KB, Urlep Ž, Lorbek G, Matz-Soja M, Skubic C, Perše M, et al. Chronic disruption of the late cholesterol synthesis leads to female-prevalent liver cancer. Cancers (Basel). 2020;12(11):1–24.

23. Sheng R, Kim H, Lee H, Xin Y, Chen Y, Tian W, et al. Cholesterol selectively activates canonical Wnt signalling over non-canonical Wnt signalling. Nat Commun. 2014;5.

24. Porter FD, Herman GE. Malformation syndromes caused by disorders of cholesterol synthesis. J Lipid Res. 2011 Jan;52(1):6–34.

25. Rohanizadegan M, Sacharow S. Desmosterolosis presenting with multiple congenital anomalies. Eur J Med Genet [Internet]. 2018;61(3):152–6. Available from: https://www.sciencedirect.com/science/article/pii/S1769721217301659

26. Rojare C, Opdenakker Y, Laborde A, Nicot R, Mention K, Ferri J. The Smith–Lemli–

Opitz syndrome and dentofacial anomalies diagnostic: Case reports and literature review. Int Orthod [Internet]. 2019;17(2):375–83. Available from: https://www.sciencedirect.com/science/article/pii/S1761722719300580

27. Rozman D, Monostory K. Perspectives of the non-statin hypolipidemic agents. Pharmacol Ther. 2010;127(1):19–40.

28. Gasteiger E, Gattiker A, Hoogland C, Ivanyi I, Appel RD, Bairoch A. ExPASy: The proteomics server for in-depth protein knowledge and analysis. Nucleic Acids Res. 2003 Jul;31(13):3784–8.

29. Skubic C, Vovk I, Rozman D, Križman M, Samples B. Simplified LC-MS Method for Analysis of Sterols in Biological Samples. Mol 2020, Vol 25, Page 4116 [Internet]. 2020;25(18):4116. Available from: https://www.mdpi.com/821784

30. Schreiber E, Harshman K, Kemler I, Malipiero U, Schaffner W, Fontana A. Astrocytes and glioblastoma cells express novel octamer-DNA binding proteins distinct from the ubiquitous Oct-1 and B cell type Oct-2 proteins. Nucleic Acids Res. 1990 Sep;18(18):5495–503.

31. Matys V, Kel-Margoulis O V, Fricke E, Liebich I, Land S, Barre-Dirrie A, et al. TRANSFAC and its module TRANSCompel: transcriptional gene regulation in eukaryotes. Nucleic Acids Res. 2006 Jan;34(Database issue):D108-10.

32. Keenan AB, Torre D, Lachmann A, Leong AK, Wojciechowicz ML, Utti V, et al. ChEA3: transcription factor enrichment analysis by orthogonal omics integration. Nucleic Acids Res [Internet]. 2019 Jul 2;47(W1):W212–24. Available from: https://doi.org/10.1093/nar/gkz446

33. Xie Z, Bailey A, Kuleshov M V, Clarke DJB, Evangelista JE, Jenkins SL, et al. Gene Set Knowledge Discovery with Enrichr. Curr Protoc [Internet]. 2021 Mar 1;1(3):e90. Available from: https://doi.org/10.1002/cpz1.90

34. Chen EY, Tan CM, Kou Y, Duan Q, Wang Z, Meirelles GV, et al. Enrichr: interactive and collaborative HTML5 gene list enrichment analysis tool. BMC Bioinformatics. 2013 Apr;14:128.

35. Aravind S, Pablo T, K. MV, Sayan M, L. EB, A. GM, et al. Gene set enrichment analysis: A knowledge-based approach for interpreting genome-wide expression profiles. Proc Natl Acad Sci [Internet]. 2005 Oct 25;102(43):15545–50. Available from: https://doi.org/10.1073/pnas.0506580102

36. Mootha VK, Lindgren CM, Eriksson K-F, Subramanian A, Sihag S, Lehar J, et al. PGC-1α-responsive genes involved in oxidative phosphorylation are coordinately downregulated in human diabetes. Nat Genet [Internet]. 2003;34(3):267–73. Available from: https://doi.org/10.1038/ng1180

37. Shannon P, Markiel A, Ozier O, Baliga NS, Wang JT, Ramage D, et al. Cytoscape: a software environment for integrated models of biomolecular interaction networks. Genome Res. 2003 Nov;13(11):2498–504.

38. Reimand J, Isserlin R, Voisin V, Kucera M, Tannus-Lopes C, Rostamianfar A, et al. Pathway enrichment analysis and visualization of omics data using g:Profiler, GSEA, Cytoscape and EnrichmentMap. Nat Protoc [Internet]. 2019;14(2):482–517. Available from: http://dx.doi.org/10.1038/s41596-018-0103-9

39. Iijima K, Yamada H, Miharu M, Imadome K-I, Miyagawa Y, Akimoto S, et al. ZNF385B

is characteristically expressed in germinal center B cells and involved in B-cell apoptosis. Eur J Immunol [Internet]. 2012 Dec 1;42(12):3405–15. Available from: https://doi.org/10.1002/eji.201242530

40. Keenan AB, Torre D, Lachmann A, Leong AK, Wojciechowicz ML, Utti V, et al. ChEA3: transcription factor enrichment analysis by orthogonal omics integration. Nucleic Acids Res. 2019;47(W1):W212–24.

41. Kanaki M, Kardassis D. Regulation of the human lipoprotein lipase gene by the forkhead box transcription factor FOXA2/HNF-3β in hepatic cells. Biochim Biophys Acta - Gene Regul Mech [Internet]. 2017;1860(3):327–36. Available from: https://www.sciencedirect.com/science/article/pii/S1874939916302589

42. Bochkis IM, Rubins NE, White P, Furth EE, Friedman JR, Kaestner KH. Hepatocyte-specific ablation of Foxa2 alters bile acid homeostasis and results in endoplasmic reticulum stress. Nat Med. 2008;14(8):828–36.

43. Yue L, Ye F, Gui C, Luo H, Cai J, Shen J, et al. Ligand-binding regulation of LXR/RXR and LXR/PPAR heterodimerizations: SPR technology-based kinetic analysis correlated with molecular dynamics simulation. Protein Sci. 2005 Mar;14(3):812–22.

44. Yoshikawa T, Ide T, Shimano H, Yahagi N, Amemiya-Kudo M, Matsuzaka T, et al. Cross-Talk between Peroxisome Proliferator-Activated Receptor (PPAR) α and Liver X Receptor (LXR) in Nutritional Regulation of Fatty Acid Metabolism. I. PPARs Suppress Sterol Regulatory Element Binding Protein-1c Promoter through Inhibition of LXR Signali. Mol Endocrinol [Internet]. 2003 Jul 1;17(7):1240–54. Available from: https://doi.org/10.1210/me.2002-0190

45. Yang C, McDonald JG, Patel A, Zhang Y, Umetani M, Xu F, et al. Sterol Intermediates from Cholesterol Biosynthetic Pathway as Liver X Receptor Ligands*. J Biol Chem [Internet]. 2006;281(38):27816–26. Available from: https://www.sciencedirect.com/science/article/pii/S0021925819580668

46. Spann NJ, Garmire LX, McDonald JG, Myers DS, Milne SB, Shibata N, et al. Regulated Accumulation of Desmosterol Integrates Macrophage Lipid Metabolism and Inflammatory Responses. Cell [Internet]. 2012;151(1):138–52. Available from: https://www.sciencedirect.com/science/article/pii/S0092867412010598

47. Heverin M, Meaney S, Brafman A, Shafir M, Olin M, Shafaati M, et al. Studies on the cholesterol-free mouse: Strong activation of LXR-regulated hepatic genes when replacing cholesterol with desmosterol. Arterioscler Thromb Vasc Biol. 2007;27(10):2191–7.

48. Reeves HL, Narla G, Ogunbiyi O, Haq AI, Katz A, Benzeno S, et al. Kruppel-like factor 6 (KLF6) is a tumor-suppressor gene frequently inactivated in colorectal cancer. Gastroenterology [Internet]. 2004;126(4):1090–103. Available from: https://www.sciencedirect.com/science/article/pii/S0016508504000253

49. Hallstrom TC, Mori S, Nevins JR. An E2F1-Dependent Gene Expression Program that Determines the Balance between Proliferation and Cell Death. Cancer Cell [Internet]. 2008;13(1):11–22. Available from: https://www.sciencedirect.com/science/article/pii/S1535610807003704

50. Dolcet X, Llobet D, Pallares J, Matias-Guiu X. NF-kB in development and progression of human cancer. Virchows Arch. 2005;446(5):475–82.

51. Gelsomino L, Gu G, Rechoum Y, Beyer AR, Pejerrey SM, Tsimelzon A, et al. ESR1

mutations affect anti-proliferative responses to tamoxifen through enhanced cross-talk with IGF signaling. Breast Cancer Res Treat [Internet]. 2016;157(2):253–65. Available from: https://doi.org/10.1007/s10549-016-3829-5

52. Zhang J, Wang X, Chen B, Suo G, Zhao Y, Duan Z, et al. Expression of Nanog gene promotes NIH3T3 cell proliferation. Biochem Biophys Res Commun [Internet]. 2005;338(2):1098–102. Available from: https://www.sciencedirect.com/science/article/pii/S0006291X05023065

53. Barclay JL, Nelson CN, Ishikawa M, Murray LA, Kerr LM, McPhee TR, et al. GH-dependent STAT5 signaling plays an important role in hepatic lipid metabolism. Endocrinology. 2011;152(1):181–92.

54. Wawryk-Gawda E, Chylińska-Wrzos P, Lis-Sochocka M, Chłapek K, Bulak K, Jędrych M, et al. P53 protein in proliferation, repair and apoptosis of cells. Protoplasma [Internet]. 2014;251(3):525–33. Available from: https://doi.org/10.1007/s00709-013-0548-1

55. Chen CL, Tsai YS, Huang YH, Liang YJ, Sun YY, Su CW, et al. Lymphoid Enhancer Factor 1 Contributes to Hepatocellular Carcinoma Progression Through Transcriptional Regulation of Epithelial-Mesenchymal Transition Regulators and Stemness Genes. Hepatol Commun. 2018;2(11):1392–407.

56. Reya T, O'Riordan M, Okamura R, Devaney E, Willert K, Nusse R, et al. Wnt Signaling Regulates B Lymphocyte Proliferation through a LEF-1 Dependent Mechanism. Immunity [Internet]. 2000;13(1):15–24. Available from: https://www.sciencedirect.com/science/article/pii/S1074761300000042

57. Hao Y-H, Lafita-Navarro MC, Zacharias L, Borenstein-Auerbach N, Kim M, Barnes S, et

al. Induction of LEF1 by MYC activates the WNT pathway and maintains cell proliferation. Cell Commun Signal [Internet]. 2019;17(1):129. Available from: https://doi.org/10.1186/s12964-019-0444-1

58. Acosta-Alvear D, Zhou Y, Blais A, Tsikitis M, Lents NH, Arias C, et al. XBP1 Controls Diverse Cell Type- and Condition-Specific Transcriptional Regulatory Networks. Mol Cell [Internet]. 2007;27(1):53–66. Available from: https://www.sciencedirect.com/science/article/pii/S1097276507004005

59. Horton JD, Goldstein JL, Brown MS. SREBPs: activators of the complete program of cholesterol and fatty acid synthesis in the liver. J Clin Invest [Internet]. 2002;109(9):1125–31. Available from: https://doi.org/10.1172/JCI15593

60. Sun F, Fu H, Liu Q, Tie Y, Zhu J, Xing R, et al. Downregulation of CCND1 and CDK6 by miR-34a induces cell cycle arrest. FEBS Lett [Internet]. 2008;582(10):1564–8. Available from: https://www.sciencedirect.com/science/article/pii/S0014579308003062

61. Baron V, Adamson ED, Calogero A, Ragona G, Mercola D. The transcription factor Egr1 is a direct regulator of multiple tumor suppressors including TGFβ1, PTEN, p53, and fibronectin. Cancer Gene Ther [Internet]. 2006;13(2):115–24. Available from: https://doi.org/10.1038/sj.cgt.7700896

62. Hoskins JW, Jia J, Flandez M, Parikh H, Xiao W, Collins I, et al. Transcriptome analysis of pancreatic cancer reveals a tumor suppressor function for HNF1A. Carcinogenesis [Internet]. 2014 Dec 1;35(12):2670–8. Available from: https://doi.org/10.1093/carcin/bgu193

63. Takeda Y, Kang HS, Freudenberg J, DeGraff LM, Jothi R, Jetten AM. Retinoic acid-

related orphan receptor γ (RORγ): a novel participant in the diurnal regulation of hepatic gluconeogenesis and insulin sensitivity. PLoS Genet. 2014;10(5):e1004331.

64. Zhang Y, Luo X, Wu D, Xu Y. ROR nuclear receptors: structures, related diseases, and drug discovery. Acta Pharmacol Sin [Internet]. 2015;36(1):71–87. Available from: https://doi.org/10.1038/aps.2014.120

65. Lou X, Meng Y, Hou Y. A literature review on function and regulation mechanism of DKK4. J Cell Mol Med [Internet]. 2021 Mar 1;25(6):2786–94. Available from: https://doi.org/10.1111/jcmm.16372

66. Gammons M, Bienz M. Multiprotein complexes governing Wnt signal transduction. Curr Opin Cell Biol [Internet]. 2018;51:42–9. Available from: https://www.sciencedirect.com/science/article/pii/S0955067417300418

67. Revollo L, Kading J, Jeong SY, Li J, Salazar V, Mbalaviele G, et al. N-cadherin restrains PTH activation of Lrp6/β-catenin signaling and osteoanabolic action. J Bone Miner Res. 2015;30(2):274–85.

68. Gu S, Liu F, Xie X, Ding M, Wang Z, Xing X, et al. β-Sitosterol blocks the LEF-1-mediated Wnt/β-catenin pathway to inhibit proliferation of human colon cancer cells. Cell Signal [Internet]. 2023;104:110585. Available from: https://www.sciencedirect.com/science/article/pii/S0898656822003473

69. Yuan L, Roy B, Ratna P, Uhler C, Shivashankar G V. Lateral confined growth of cells activates Lef1 dependent pathways to regulate cell-state transitions. Sci Rep [Internet]. 2022;12(1):17318. Available from: https://doi.org/10.1038/s41598-022-21596-4

70. Jost PJ, Ruland J. Aberrant NF-kappaB signaling in lymphoma: mechanisms,

consequences, and therapeutic implications. Blood. 2007 Apr;109(7):2700–7.

71. Yun K, Choi YD, Nam JH, Park Z, Im S-H. NF-κB regulates Lef1 gene expression in chondrocytes. Biochem Biophys Res Commun [Internet]. 2007;357(3):589–95. Available from: https://www.sciencedirect.com/science/article/pii/S0006291X0700602X

72. Massagué J, Seoane J, Wotton D. Smad transcription factors. Genes Dev. 2005 Dec;19(23):2783–810.

73. Letamendia A, Labbé E, Attisano L. Transcriptional Regulation by Smads: Crosstalk between the TGF-β and Wnt Pathways. JBJS [Internet]. 2001;83(1). Available from: https://journals.lww.com/jbjsjournal/Fulltext/2001/00001/Transcriptional_Regulation_by_Smads__Crosstalk.5.aspx

74. Huang F-I, Chen Y-L, Chang C-N, Yuan R-H, Jeng Y-M. Hepatocyte growth factor activates Wnt pathway by transcriptional activation of LEF1 to facilitate tumor invasion. Carcinogenesis [Internet]. 2012 Jun 1;33(6):1142–8. Available from: https://doi.org/10.1093/carcin/bgs131

75. Ačimovič J, Rozman D. Steroidal triterpenes of cholesterol synthesis. Molecules. 2013;18(4):4002–17.

76. Mitsche MA, McDonald JG, Hobbs HH, Cohen JC. Flux analysis of cholesterol biosynthesis in vivo reveals multiple tissue and cell-type specific pathways. Elife. 2015;4:1–21.

77. Keber R, Motaln H, Wagner KD, Debeljak N, Rassoulzadegan M, Ačimovič J, et al. Mouse knockout of the cholesterogenic cytochrome P450 lanosterol 14alpha-demethylase (Cyp51) resembles Antley-Bixler syndrome. J Biol Chem. 2011 Aug;286(33):29086–97.

78. Lorbek G, Perše M, Jeruc J, Juvan P, Gutierrez-Mariscal FM, Lewinska M, et al. Lessons from Hepatocyte-Specific Cyp51 Knockout Mice: Impaired Cholesterol Synthesis Leads to Oval Cell-Driven Liver Injury. Sci Rep. 2015;5:1–11.

79. Sax JL, Hubler Z, Allimuthu D, Adams DJ. Screening Reveals Sterol Derivatives with Pro-Differentiation, Pro-Survival, or Potent Cytotoxic Effects on Oligodendrocyte Progenitor Cells. ACS Chem Biol. 2021;16(7):1288–97.

80. Mohammad N, Malvi P, Meena AS, Singh SV, Chaube B, Vannuruswamy G, et al. Cholesterol depletion by methyl-β-cyclodextrin augments tamoxifen induced cell death by enhancing its uptake in melanoma. Mol Cancer [Internet]. 2014;13(1):204. Available from: https://doi.org/10.1186/1476-4598-13-204

81. Portilho DM, Soares CP, Morrot A, Thiago LS, Butler-Browne G, Savino W, et al. Cholesterol depletion by methyl-β-cyclodextrin enhances cell proliferation and increases the number of desmin-positive cells in myoblast cultures. Eur J Pharmacol [Internet]. 2012;694(1):1–12. Available from: https://www.sciencedirect.com/science/article/pii/S0014299912006772

82. Matsumura I, Tanaka H, Kanakura Y. E2F1 and c-Myc in cell growth and death. Cell Cycle. 2003;2(4):332–5.

83. Kanehisa M, Goto S. KEGG: kyoto encyclopedia of genes and genomes. Nucleic Acids Res. 2000 Jan;28(1):27–30.

Figures legends

Figure 1. Expression of mRNA and proteins in control HepG2 cells (Native) and in knockout cells of enzymes from the late part of cholesterol synthesis (*CYP51* KO, *DHCR24* KO, *SCD* KO). Bars represent the mean + SD of three measurements. **A – C:** Relative mRNA expression of targeted genes (**A** - *CYP51*, **B** - *DHCR24*, **C** - *SC5D*). Expression data was normalized to *ACTB*, *GAPDH*, and *RPLP0* reference genes. **D** - **I**: Targeted protein expression (**D** - CYP51A1, **E** - DHCR24, **F** - SC5D, **G –** HMGCR**, H –** c-SREBP2**, I –** n-SREBP2), by western blotting and appropriate antibody as described in Methods. 10 µg of proteins were loaded and normalized to total proteins. **J)** Sterol analysis by LC-MS. Sterol concentrations are represented as a mean +/- SD in ng/10^7 cells, except for cholesterol in µg/10^7 cells. The colours represent relative concentration compared to Native cells (Blue – Depleted; Red – Accumulated), ND – non-detectable, N=3. Cholesterol* in KO cells results from the culture medium. **K)** A simplified cholesterol synthesis, with measured sterols from the post-lanosterol part of a synthesis and the position of deleted enzymes in red. The Bloch and Kandutsch-Russell sterol pathways are indicated. For statistics, one-way ANOVA was used. *p<0.1, **p<0.05, ***p<0.01, ****p<0.001.

Figure 2. Differential gene expression (DEG) using Clarium S microarrays. **A)** PCA (Principal component analysis) of raw gene expression data for all four conditions (Native, *CYP51* KO, *DHCR24* KO, and *SC5D* KO), each measurement in 3 biological replicates. **B)** Number of up, down, and total differently expressed genes in all three genotypes compare to the Native HepG2 cell line after False discovery rate (FDR) correction (adj pvalue<0.05). **C)** Venn diagram of DEGs comparing gene expression between different genotypes. **D)** Venn diagram of changed KEGG pathways comparing different genotypes. **E)** (*CYP51* KO), **F)** (*DHCR24* KO) and **G)**

(*SC5D* KO) represent volcano plots of differentially expressed genes, downregulated shown in blue and upregulated in red (FDR<0.05). The top 10 statistically significant genes are labelled. **H)** (*CYP51* KO), **I)** (*DHCR24* KO) and **J)** (*SC5D* KO) represent changes in KEGG metabolic pathways (FDR<0.05), with red showing the pathways that are upregulated and blue those that are downregulated. The # after the pathway name indicates significant change unique for this KOs cell line.

Figure 3. Transcription factor enrichment analysis using ChEA 2022 and TransFac 2.0 . **A)** The top 20 enriched TFs from each KO cell line were used for visualization of ChEA data. **B)** The Venn diagram of enriched TFs from ChEA analysis, **C)** TFs significantly enriched in TransFac 2.0 analysis. **D)** The Venn diagram of enriched TFs from TransFac 2.0 analysis. How many TFs are in each group is represented with a number and % indicates the fraction of all TFs in this analysis. m.i. - muscle initiator.

Figure 4. Proliferation and cell cycle analysis of HepG2 cell lines. Plots represent the proliferation of HepG2 cell lines in different serum and cholesterol conditions on **A)** FBS**, B)** LDS + 30 µg/ml cholesterol and **C) LDS**. The assay was performed using the CCK8 method and data are represented as mean +/- SE (n=6). Statistical significance was tested using One-way ANOVA with comparison to control, the Native cell line result at the same time point, p-value - *< 0.05, **< 0.01, ***< 0.001, ****<0.0001. Cell cycle measurements using propidium iodide are represented on **D)** as a direct measurement and on **E)** results normalized to total cell number (100%) and statistically evaluated. All KOs were compared with control Native cell line using the statistical test described above.

Figure 5. Activation of the WNT signalling pathway and unchanged RORC. A) Heat map of genes, measured with microarrays, that are known targets of RORC; B) Heat map of genes from the WNT signalling pathway (obtained from the KEGG database (83)) measured with microarrays. On both heat maps, white represents genes that are not changed after statistical testing, blue are downregulated and red are upregulated genes, with colour intensity representing fold change. C) WNT genes measured by RT-qPCR - data are represented as mean +/- SD (n=3). D) Expression of proteins from the WNT signalling pathway analysed using Western Blots in E). Statistical significance was tested using One-way ANOVA with comparison to control, the Native cell line result at the same time point. p-value - *< 0.05, **< 0.01, ***< 0.001, ****<0.0001.

Figure 6. Possible activation of WNT and NF-kB signalling pathways by 24,25-dihydrolansterol accumulation. The Figure represents two of the most probable signalling pathways NFKB and WNT that upon 24,25-dihydrolansterol accumulation caused elevation of LEF1.

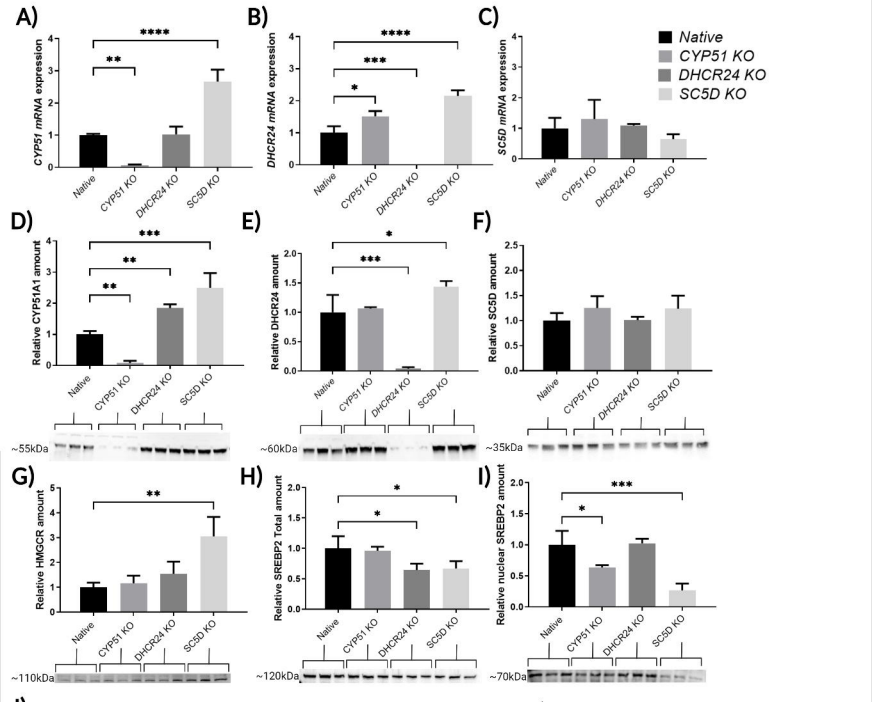

J)

Sterol (ng/10^7 cells)	GENOTYPE			
	NATIVE	CYP51 KO	DHCR24 KO	SC5D KO
Lanosterol	41.62 ± 1.4	1277.6 ± 63.2	120.9 ± 1.9	27.7 ± 12.5
Dihydrolanosterol	19.4 ± 2.7	31086.2 ± 1042.9	ND	13.3 ± 9.7
T-MAS	89.55 ± 7.6	ND	621.5 ± 26.3	59.7 ± 10.6
FF-MAS	ND	ND	ND	ND
Zymosterol	98.5 ± 4.6	ND	939.0 ± 94.2	77.7 ± 13.0
Zymostenol	184.4 ± 5.8	16.8 ± 2.1	12.4 ± 2.0	1515.1 ± 277.1
24-dehydrolathosterol	30.6 ± 3.1	ND	539.6 ± 28.2	48.9 ± 12.5
Lathosterol	351.8 ± 17.9	ND	ND	27335.4 ± 5758.4
7-dehydrodesmosterol	10.5 ± 1.3	ND	546.6± 38.4	ND
Desmosterol	133.9 ± 5.0	ND	42339.4 ± 2385.3	ND
Cholesterol*	135.9 ± 3.0	56.7 ± 3.85	44.6 ± 2.8	63.9 ± 11.6

Depletion — Normal — Accumulation

K)

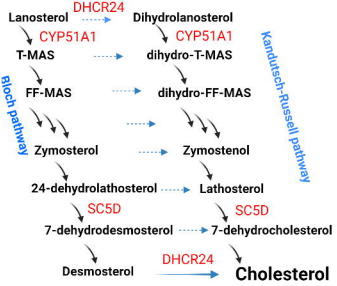

A)

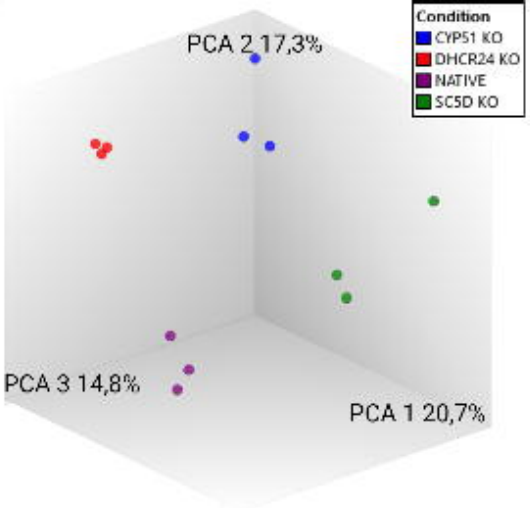

B)

Genotype	Differentialy expressed genes (adj pvalue < 0.05)		
	Up	Down	Total
CYP51 KO	185	226	411
DHCR24 KO	219	323	542
SC5D KO	411	354	765

C) Differentially expressed genes

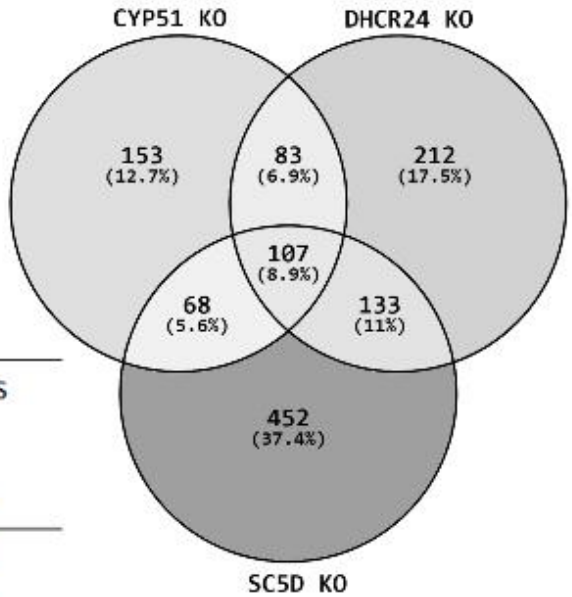

D) KEGG Pathways

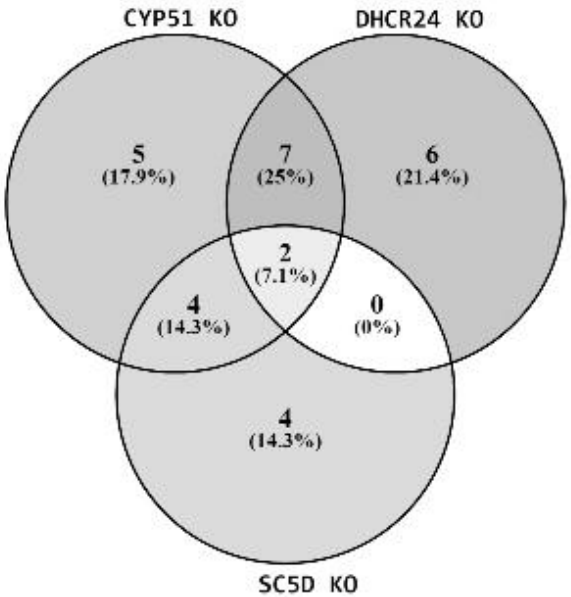

E)

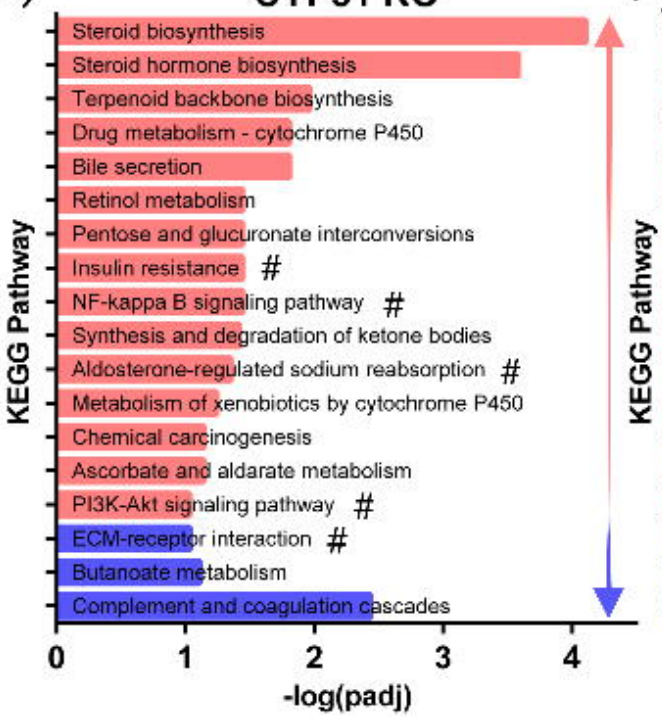

F)

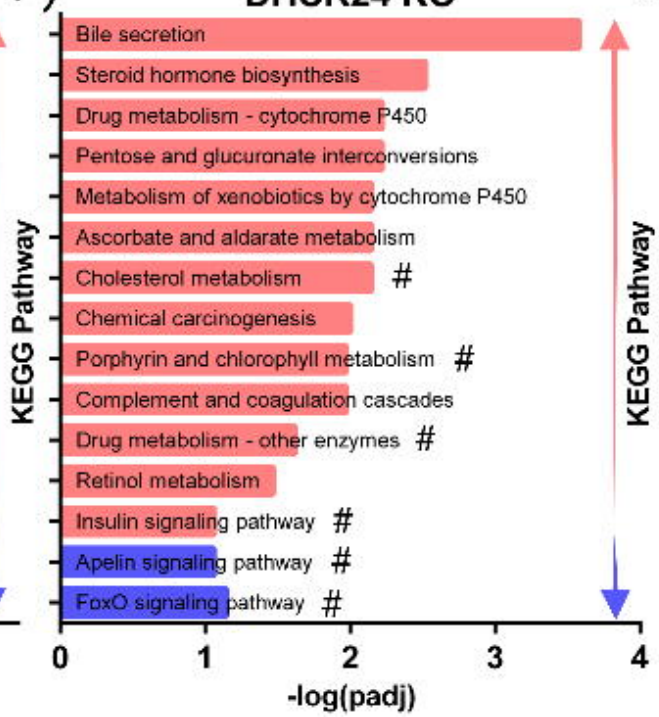

G)

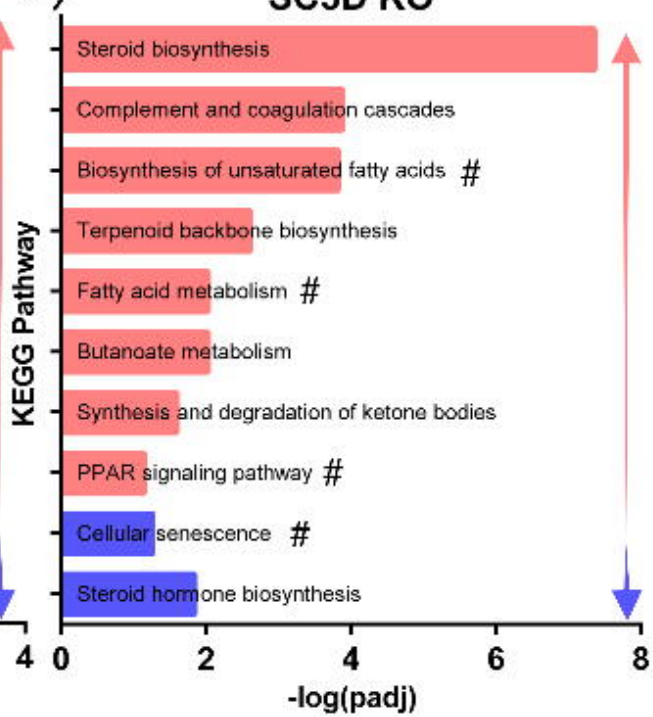

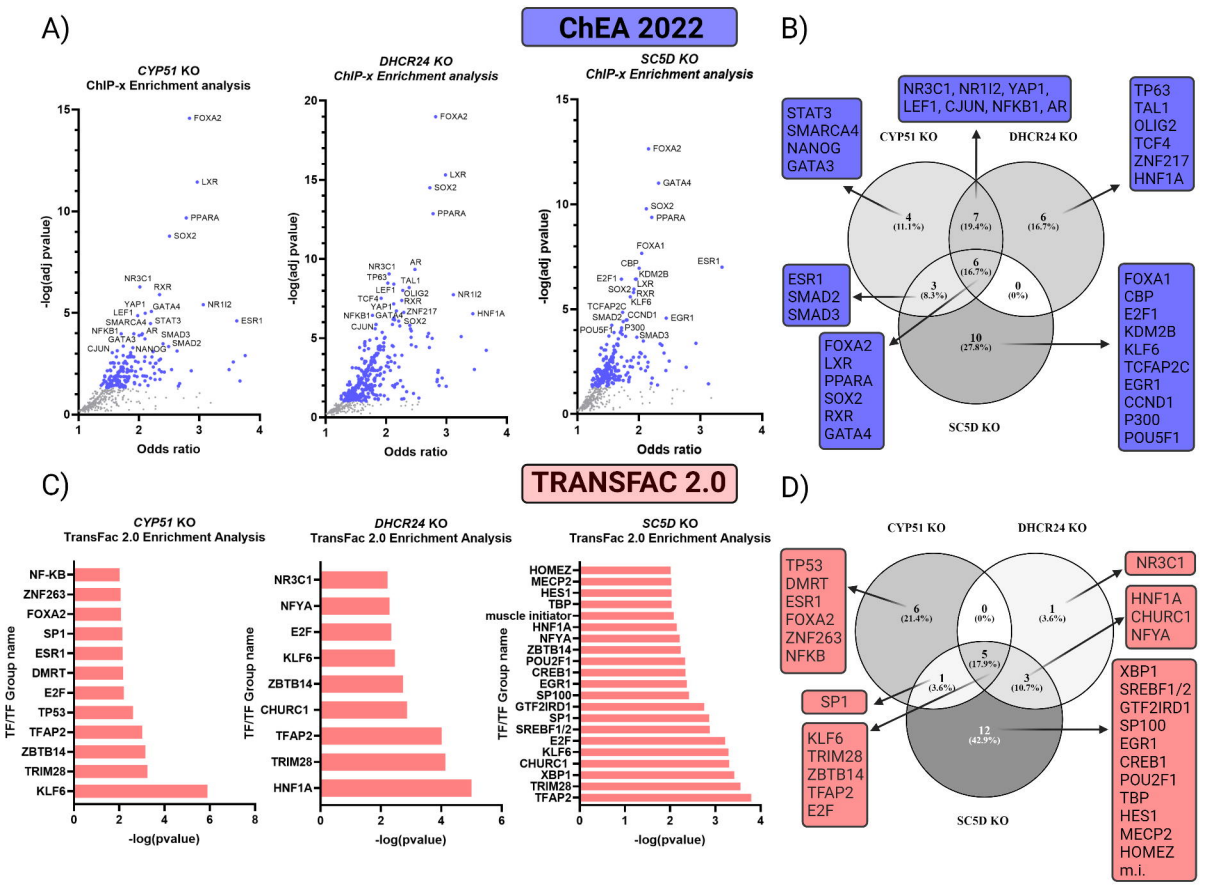
A)
ChEA 2022
CYP51 KO
ChIP-x Enrichment analysis
DHCR24 KO
ChIP-x Enrichment analysis
SC5D KO
ChIP-x Enrichment analysis
-log(adj pvalue)
Odds ratio
FOXA2
LXR
PPARA
SOX2
NR3C1
RXR
YAP1
GATA4
NR1I2
LEF1
STAT3
SMARCA4
ESR1
NFKB1
AR
SMAD3
GATA3
SMAD2
CJUN
NANOG
TP63
TAL1
OLIG2
TCF4
ZNF217
HNF1A
CJUN2
GATA4
CBP
KDM2B
E2F1
KLF6
TCFAP2C
SMAD2
CCND1
EGR1
POU5F1
P300
B)
NR3C1, NR1I2, YAP1, LEF1, CJUN, NFKB1, AR
STAT3
SMARCA4
NANOG
GATA3
TP63
TAL1
OLIG2
TCF4
ZNF217
HNF1A
CYP51 KO
DHCR24 KO
4 (11.1%)
7 (19.4%)
6 (16.7%)
6 (16.7%)
3 (8.3%)
0 (0%)
10 (27.8%)
ESR1
SMAD2
SMAD3
FOXA2
LXR
PPARA
SOX2
RXR
GATA4
FOXA1
CBP
E2F1
KDM2B
KLF6
TCFAP2C
EGR1
CCND1
P300
POU5F1
SC5D KO
C)
TRANSFAC 2.0
CYP51 KO
TransFac 2.0 Enrichment Analysis
DHCR24 KO
TransFac 2.0 Enrichment Analysis
SC5D KO
TransFac 2.0 Enrichment Analysis
TF/TF Group name
-log(pvalue)
NF-KB
ZNF263
FOXA2
SP1
ESR1
DMRT
E2F
TP53
TFAP2
ZBTB14
TRIM28
KLF6
NR3C1
NFYA
E2F
KLF6
ZBTB14
CHURC1
TFAP2
TRIM28
HNF1A
HOMEZ
MECP2
HES1
TBP
muscle initiator
HNF1A
NFYA
ZBTB14
POU2F1
CREB1
EGR1
SP100
GTF2IRD1
SP1
SREBF1/2
E2F
KLF6
CHURC1
XBP1
TRIM28
TFAP2
D)
CYP51 KO
DHCR24 KO
TP53
DMRT
ESR1
FOXA2
ZNF263
NFKB
6 (21.4%)
0 (0%)
1 (3.6%)
5 (17.9%)
1 (3.6%)
3 (10.7%)
12 (42.9%)
NR3C1
HNF1A
CHURC1
NFYA
SP1
KLF6
TRIM28
ZBTB14
TFAP2
E2F
XBP1
SREBF1/2
GTF2IRD1
SP100
EGR1
CREB1
POU2F1
TBP
HES1
MECP2
HOMEZ
m.i.
SC5D KO

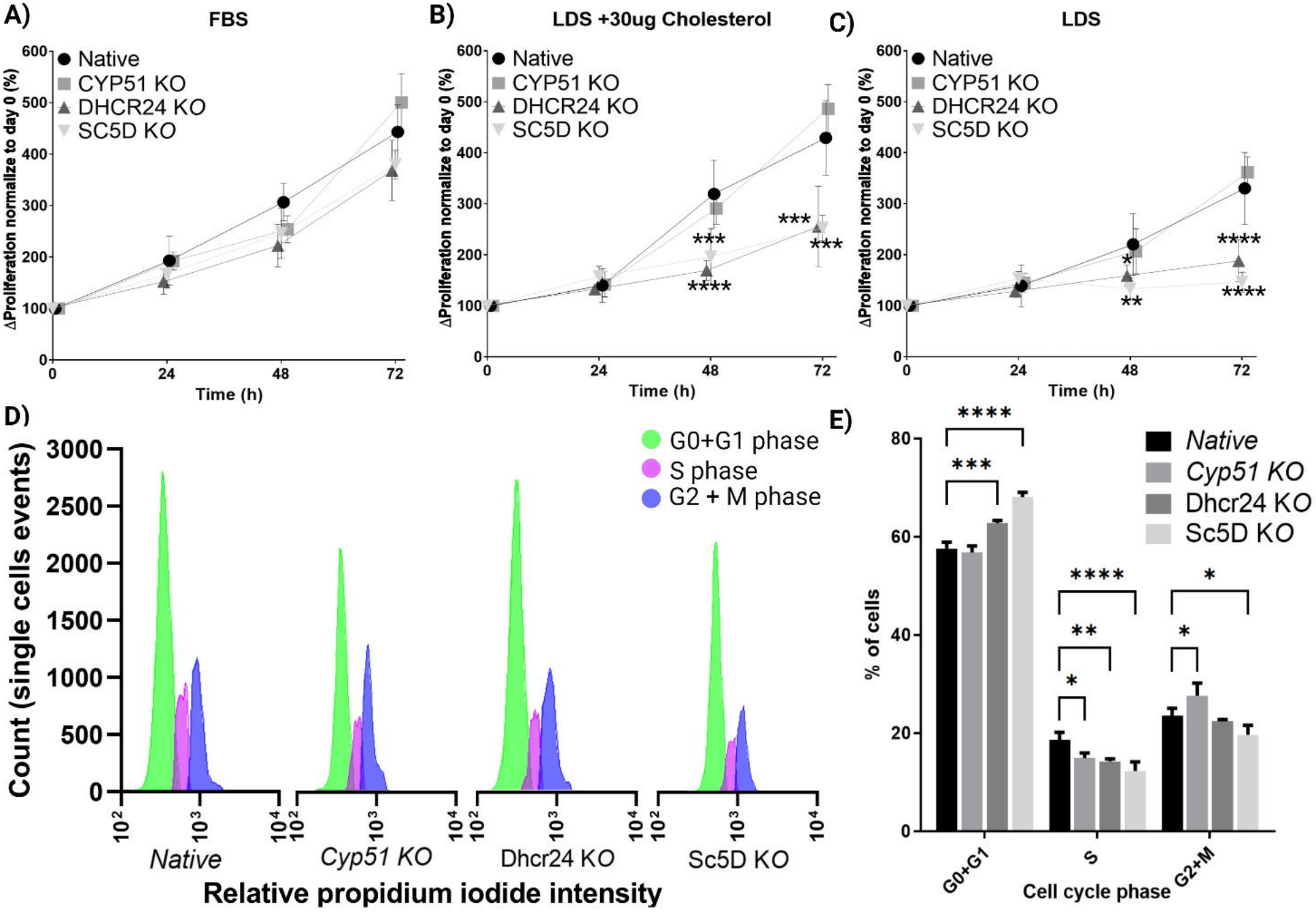
A)
FBS
Native
CYP51 KO
DHCR24 KO
SC5D KO
ΔProliferation normalize to day 0 (%)
Time (h)
B)
LDS +30ug Cholesterol
C)
LDS
D)
G0+G1 phase
S phase
G2 + M phase
Count (single cells events)
Native
Cyp51 KO
Dhcr24 KO
Sc5D KO
Relative propidium iodide intensity
E)
Native
Cyp51 KO
Dhcr24 KO
Sc5D KO
% of cells
G0+G1
S
G2+M
Cell cycle phase

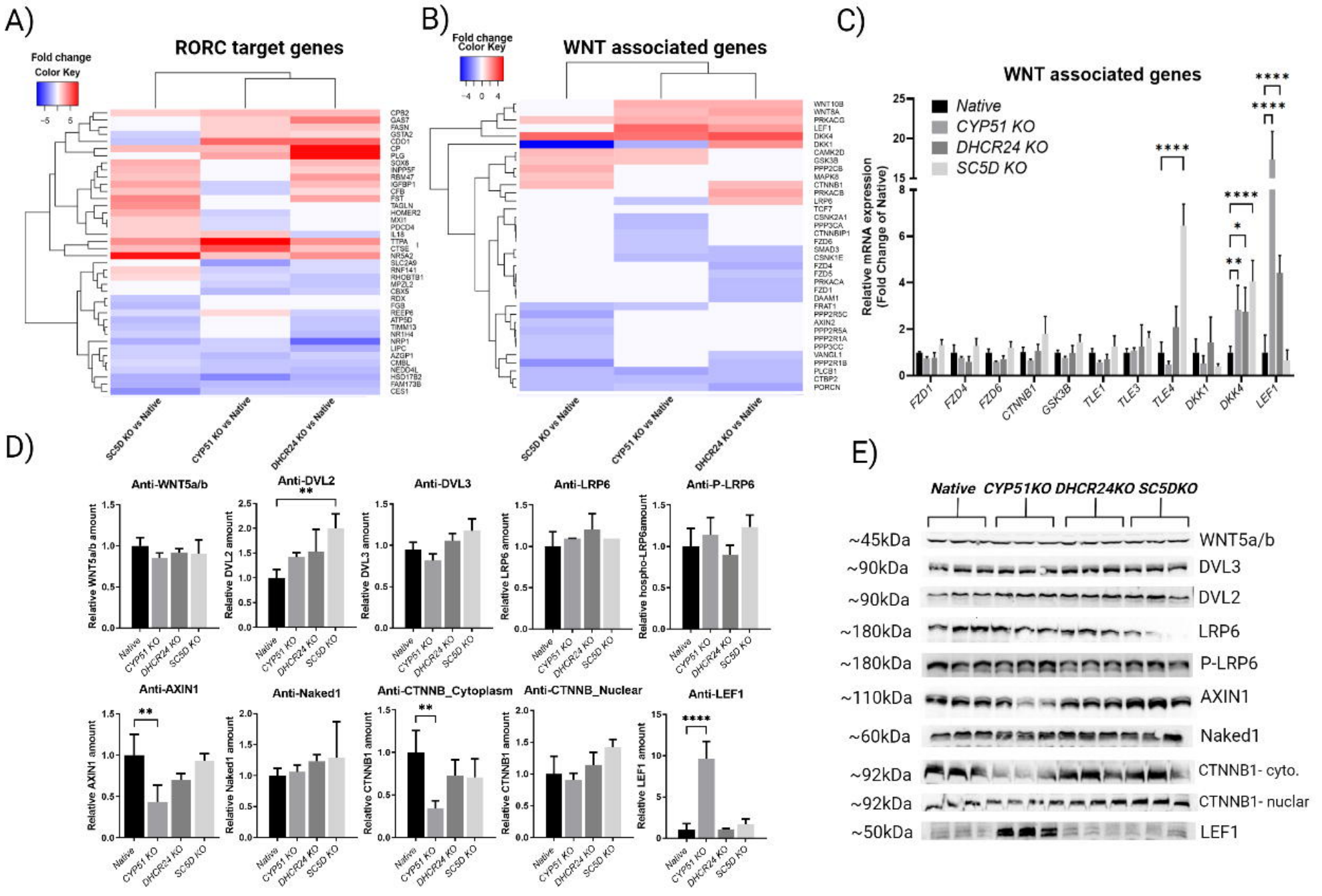
A)
RORC target genes
Fold change
Color Key
-5
5
CPB2
GAS7
FASN
GSTA2
CDO1
CP
PLG
SOX6
INPP5F
RBM47
IGFBP1
CFB
FST
TAGLN
HOMER2
MXI1
PDCD4
IL18
TTPA
CTSE
NR5A2
SLC2A9
RNF141
RHOBTB1
MPZL2
CBX5
RDX
FGB
REEP6
ATP5D
TIMM13
NR1H4
NRP1
LIPC
AZGP1
CMBL
NEDD4L
HSD17B2
FAM173B
CES1
SC5D KO vs Native
CYP51 KO vs Native
DHCR24 KO vs Native
B)
WNT associated genes
Fold change
Color Key
-4
0
4
WNT10B
WNT8A
PRKACG
LEF1
DKK4
DKK1
CAMK2D
GSK3B
PPP2CB
MAPK8
CTNNB1
PRKACB
LRP6
TCF7
CSNK2A1
PPP3CA
CTNNBIP1
FZD6
SMAD3
CSNK1E
FZD4
FZD5
PRKACA
FZD1
DAAM1
FRAT1
PPP2R5C
AXIN2
PPP2R5A
PPP2R1A
PPP3CC
VANGL1
PPP2R1B
PLCB1
CTBP2
PORCN
SC5D KO vs Native
CYP51 KO vs Native
DHCR24 KO vs Native
C)
WNT associated genes
Native
CYP51 KO
DHCR24 KO
SC5D KO
Relative mRNA expression
(Fold Change of Native)
FZD1
FZD4
FZD6
CTNNB1
GSK3B
TLE1
TLE3
TLE4
DKK1
DKK4
LEF1
D)
Anti-WNT5a/b
Anti-DVL2
Anti-DVL3
Anti-LRP6
Anti-P-LRP6
Anti-AXIN1
Anti-Naked1
Anti-CTNNB_Cytoplasm
Anti-CTNNB_Nuclear
Anti-LEF1
Relative WNT5a/b amount
Relative DVL2 amount
Relative DVL3 amount
Relative LRP6 amount
Relative hospho-LRP6amount
Relative AXIN1 amount
Relative Naked1 amount
Relative CTNNB1 amount
Relative CTNNB1 amount
Relative LEF1 amount
Native
CYP51 KO
DHCR24 KO
SC5D KO
E)
Native
CYP51KO
DHCR24KO
SC5DKO
~45kDa
WNT5a/b
~90kDa
DVL3
~90kDa
DVL2
~180kDa
LRP6
~180kDa
P-LRP6
~110kDa
AXIN1
~60kDa
Naked1
~92kDa
CTNNB1- cyto.
~92kDa
CTNNB1- nuclar
~50kDa
LEF1

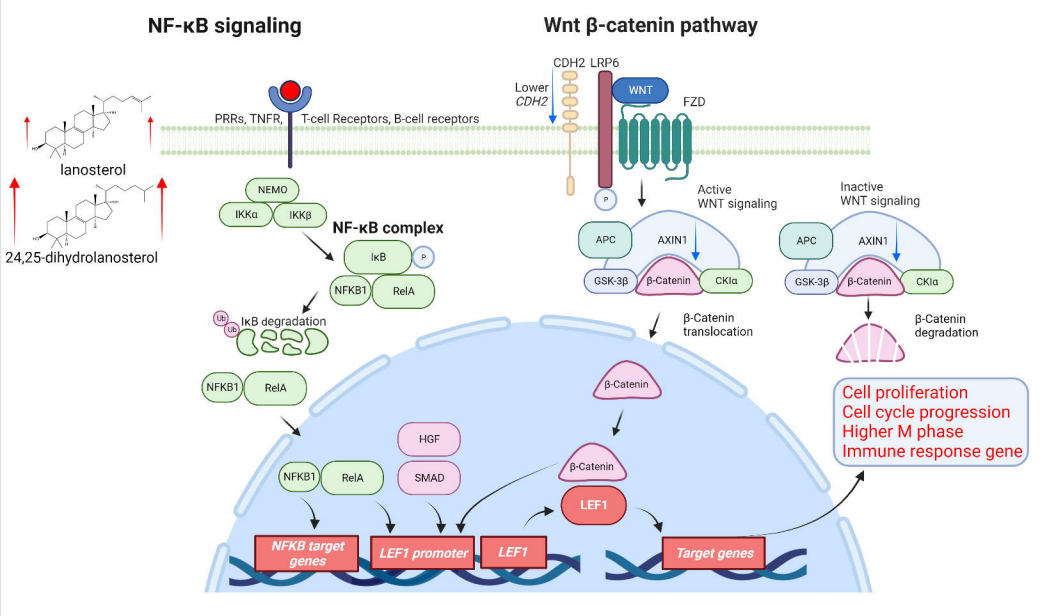
NF-κB signaling
Wnt β-catenin pathway
lanosterol
24,25-dihydrolanosterol
PRRs, TNFR, T-cell Receptors, B-cell receptors
NEMO
IKKα
IKKβ
NF-κB complex
IκB
P
NFKB1
RelA
Ub
IκB degradation
NFKB1
RelA
HGF
SMAD
NFKB1
RelA
NFKB target genes
LEF1 promoter
LEF1
CDH2
LRP6
Lower CDH2
WNT
FZD
P
Active WNT signaling
APC
AXIN1
GSK-3β
β-Catenin
CKIα
β-Catenin translocation
β-Catenin
β-Catenin
LEF1
Target genes
Inactive WNT signaling
APC
AXIN1
GSK-3β
β-Catenin
CKIα
β-Catenin degradation
Cell proliferation
Cell cycle progression
Higher M phase
Immune response gene